Supplementary Information

Ultimate design principles and fabrication process for high-energy-density solid-state pouch cells based on solid polymer electrolytes

Wonmi Lee[a,†], Taegyun Yu[a,†], Juho Lee[a,b], Sungbin Jang[a], Juhee Kim[a], Yujin Han[a], Sunghun Choi[c], Sinho Choi[a], Taehee Kim[a], Sang-Hoon Park[a], Wooyoung Jin[a], Gyujin Song[a], Daeil Kim[d], Bo-Yun Jang[d], Dong-Hwa Seo[b], Sung-Kyun Jung[*,b], Jinsoo Kim[*,a]

[a] Ulsan Advanced Energy Technology R&D Center, Korea Institute of Energy Research, Ulsan, Republic of Korea

[b] Department of Energy Engineering, School of Energy and Chemical Engineering, Ulsan National Institute of Science and Technology (UNIST), Ulsan, Republic of Korea

[c] Gwangju Clean Energy Research Center, Korea Institute of Energy Research, Gwangju, Republic of Korea

[d] Energy Storage Laboratory, Korea Institute of Energy Research, Daejeon, Republic of Korea

* Email addresses of corresponding authors.

Tel: +82-52-702-2534, jkim@kier.re.kr (J. Kim)

Tel: +82-52-217-3030, skjung@unist.ac.kr (S.-K. Jung)

Keywords: solid-state batteries; electrode density; isostatic press; electrode–solid electrolyte composite design; energy density

Supplementary Note 1. Calculation of ionic ASR of the particle composing the composite cathode

For calculation of the ionic ASR of the particle composing the composite cathode, there is the assumption that the particle has a core–shell structure. Here, the core and shell consist of the AM and SE, respectively.

Equation (1):

$$R = \rho \frac{l}{A}$$

(Here, R is the ionic ASR of the particle, ρ is the density of the particle, l is the length of the particle, and A is the area of the particle.)

Equation (2):

$$dR = \rho \frac{dl}{dA} = \rho \frac{r\, d\theta}{2\pi r\, sin\theta\, dr} = \frac{\rho\, d\theta}{2\pi\, sin\theta\, dr}$$

(Here, r is the radius of the particle, θ is the angle between the radius and the core–surface distance.)

Equation (3):

$$dR = \frac{\rho}{2\pi\,(r_2 - r_1)} \frac{d\theta}{sin\theta} = \frac{\rho}{2\pi\,(r_2 - r_1)} \int_{\theta}^{\pi-\theta} \frac{d\theta}{sin\theta}$$

(Here, r_2 is the radius of the core–shell particle, r_2 is the radius of the core side.)

Equation (4):

$$R = \frac{1}{2\pi\sigma\,(r_2 - r_1)} \ln\left(\frac{1 + cos\theta}{1 - cos\theta}\right)$$

$$= \frac{1}{2\pi\sigma\,(r_2 - r_1)} \ln\left(\frac{r_2 + r_2 cos\theta}{r_2 - r_2 cos\theta}\right)$$

$$= \frac{1}{2\pi\sigma\,(r_2 - r_1)} \ln\left(\frac{r_2 + x}{r_2 - x}\right)$$

(Here, x is the core–surface distance, which is $r_2 cos\theta$. $0 < \theta < \frac{\pi}{2}, 0 < r_2 cos\theta < 1$.)

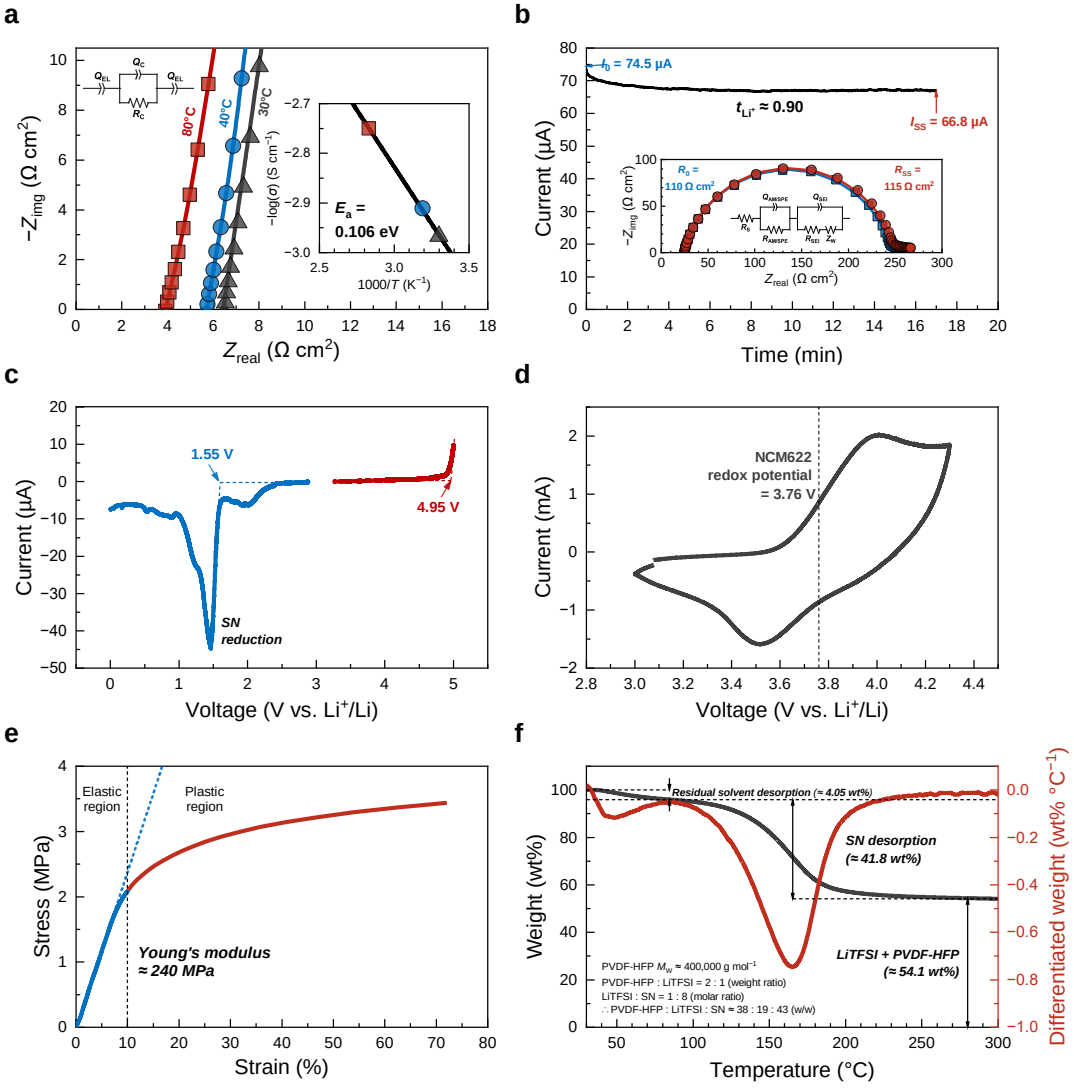

Supplementary Fig. 1: Properties and electrochemical performance of freestanding solid polymer electrolyte

a, EIS data of SS/SPE/SS coin cell and Arrhenius plot for calculation of the activation energy of the SPE. **b,** EIS and CA results of Li/SPE/Li coin cell for calculation of the lithium-ion transference number. **c,** LSV curve of Li/SPE/SS coin cell to show electrochemical stable window. **d,** CV curve of Li/SPE/NCM622 coin cell to show the redox potential of NCM622 as an AM in the cathode. **e,** DMA result showing the mechanical strength of the SPE. **f,** TGA curve showing the thermal stability of the SPE.

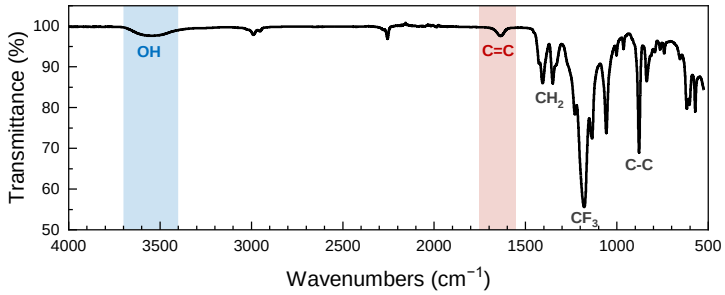

Supplementary Fig. 2: FTIR data of SPE (consisting of PVDF-HFP as the polymer matrix, LiTFSI as the Li salt, and SN as a plasticizer).

The partial dehydrofluorination of PVDF-HFP can improve the mobility of ions, leading to high ionic conductivity, as proven by the appearance of hydroxyl and C=C double bonds in the FTIR data[S1].

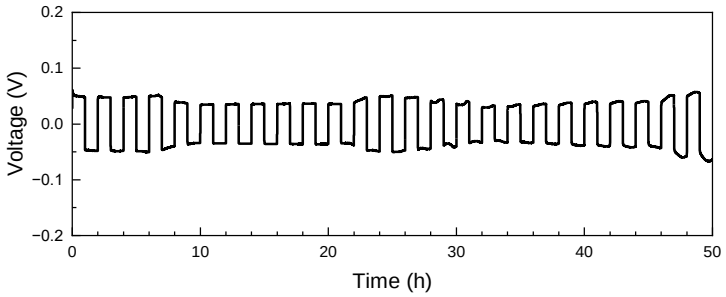

Supplementary Fig. 3: Li symmetric cycling result of Li/SPE/Li coin cell with current density of ±0.15 mA cm−2 for 1 h as each cycle.

The compatibility of the SPE and Li-metal anode was identified by Li symmetric cycling testing. The SPE showed stable cycling with Li metal, indicating that it is compatible with a Li-metal anode.

Supplementary Note 2. Calculation of electrode porosity of composite cathode

Equation (5):

$$\text{Electrode porosity} = \frac{1 - electrode\ density}{\frac{Wt_{AM+SE}}{\left(\frac{Wt_{AM}}{true\ density_{AM}}\right) + \left(\frac{Wt_{SE}}{true\ density_{SE}}\right)}} \times 100$$

Here, the electrode porosity is the volumetric porosity of the electrode [vol%], and the $electrode\ density$ is the apparent density of the electrode [g cm^{-3}], Wt_{AM+SE} is the total weight fraction of the AM and SE [wt%], Wt_{AM} is the weight fraction of the AM [wt%], Wt_{SE} is the weight fraction of the SE [wt%], $true\ density_{AM}$ is the true density of the AM [g cm^{-3}], and $true\ density_{SE}$ is the true density of the SE [g cm^{-3}].

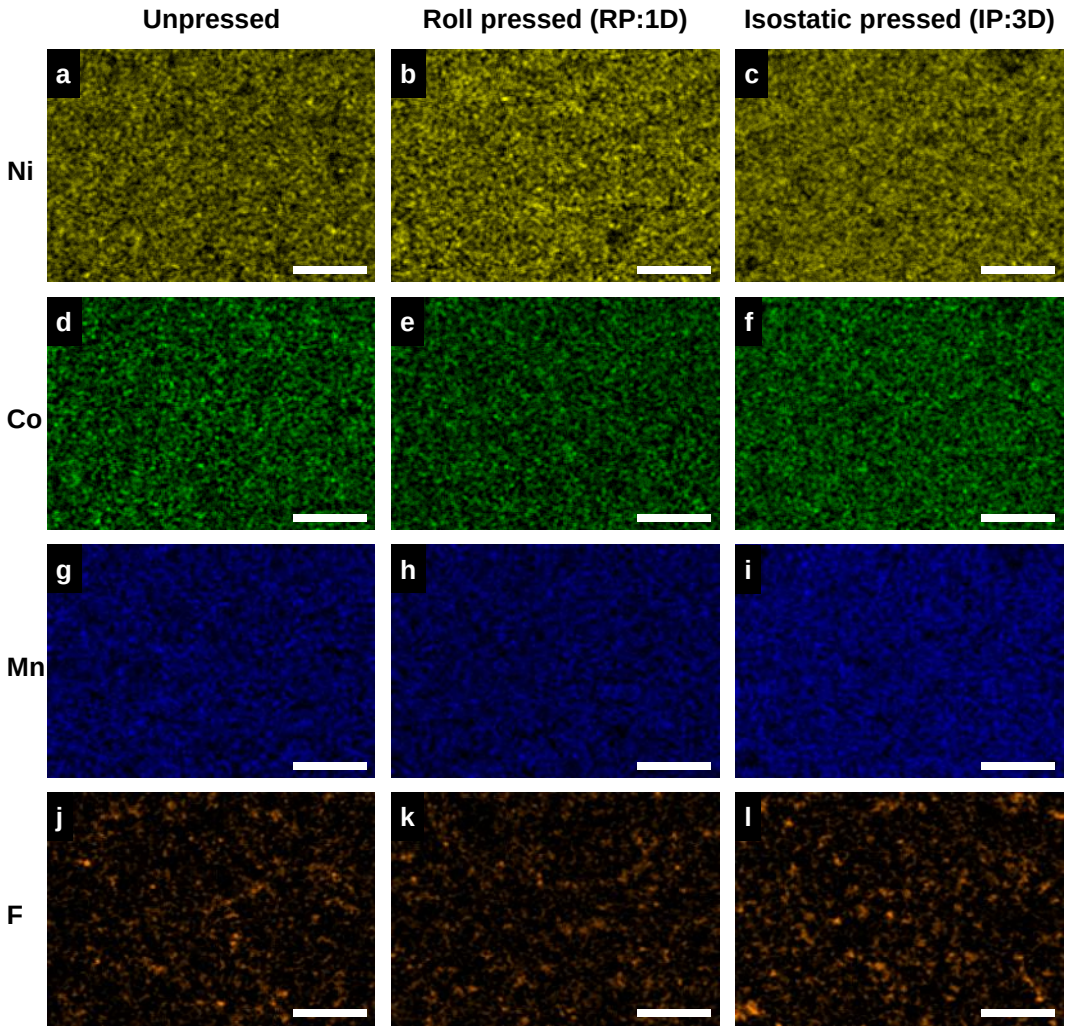

Supplementary Fig. 4: EDS data of cathodes prepared using different pressing methods (**a,** unpressed, **b,** roll-pressed, and **c,** isostatic-pressed methods. The scale bars are 100 μm.).

The EDS analysis focused on Ni, Co, Mn, and F atoms because NCM622 consists of Ni, Co, and Mn atoms, and PVDF-HFP in the binder consists of F atoms. The Ni, Co, Mn, and F atoms were uniformly distributed in the cathode, demonstrating the cathode uniformity.

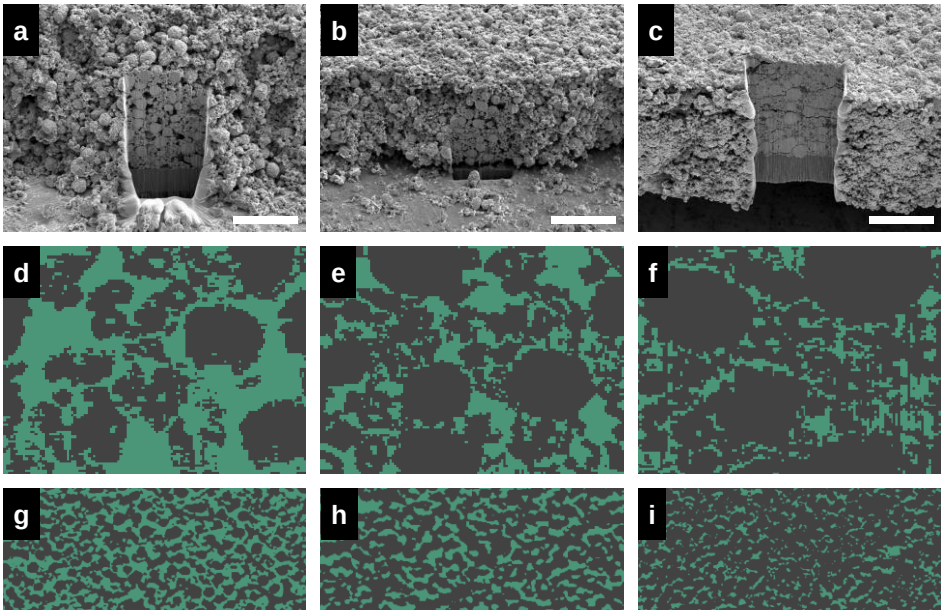

Supplementary Fig. 5: 3D and 2D FIB and X-ray CT images of the cathodes prepared using different pressing methods

3D view of FIB image of cathodes prepared using (**a**) unpressed, (**b**) roll-pressed, and (**c**) isostatic-pressed methods. 2D FIB images of cathodes prepared using (**d**) unpressed, (**e**) roll-pressed, and (**f**) isostatic-pressed methods (the green and black colors indicate voids and AM, respectively.). 2D X-ray CT image of cathodes prepared using (**g**) unpressed, (**h**) roll-pressed, and (**i**) isostatic-pressed methods (the green and black colors indicate voids and AM, respectively. The scale bars are 50 μm.).

In the FIB results, the cathode prepared using the WIP method also showed the lowest electrode porosity with reduced voids. Moreover, according to the X-ray CT analysis of the cathodes prepared using different compressing methods, the cathode prepared using the WIP method showed the lowest electrode porosity and highest electrode density. In summary, the WIP method is efficient for preparing ideal cathodes with low electrode porosity and high electrode density, leading to the formation of uniform and desirable interfacial contact with lowered resistance of the electrode.

Supplementary Note 3. Calculation of the cathode IR drop of SSBs

Equation (6):

$$\text{IR drop} = Q_{AM,sp} \times \frac{cathode\ loading\ thickness}{2 \times r_{AM,sp}} \times ASR \times \frac{cathode\ loading\ thickness}{2 \times r_{AM,sp}} \times C - rate$$

Here, IR drop is the voltage drop [mV]; $Q_{AM,sp}$ is the areal specific capacity of a single particle of AM [mAh cm^{-2}], which can be calculated using **Equation (13)**; the $cathode\ loading\ thickness$ [cm] can be calculated by dividing the areal cathode loading by the electrode density; $r_{AM,sp}$ is the radius of a single particle of AM [cm]; ASR is the areal specific resistance of the composite [Ohm cm^2], which can be calculated using **Equation (1)**; and $C - rate$ is the rate at which the battery is providing energy [C = 1/h].

Equation (7):

$$Q_{AM,sp} = \frac{Q_{AM} \times true\ density_{AM} \times V_{AM,sp}}{A_{composite}}$$

Here, $Q_{AM,sp}$ is the areal specific capacity of a single particle of AM [mAh cm^{-2}]; Q_{AM} is the specific capacity of the AM [mAh g^{-1}]; $true\ density_{AM}$ is the material true density of the AM [g cm^{-3}]; $V_{AM,sp}$ is the volume of a single particle of AM [cm^3], which can be calculated by **Equation (14)**; and $A_{composite}$ is the area of the composite consisting of the AM and SE [cm^2], which can be calculated using **Equation (15)**.

Equation (8):

$$V_{AM,sp} = \frac{4}{3}\pi \times (r_{AM,sp})^3$$

Equation (9):

$$A_{composite} = \pi \times (r_{AM,sp} + t_{squized\ SE})^2$$

Here, $t_{squized\ SE}$ is the squized thickness of SE [cm].

Equation (10):

$$\mathrm{ASR} = \ln\left(\frac{\left(r_{AM} + t_{squized\ SE}\right) + r_{AM}}{\left(r_{AM} + t_{squized\ SE}\right) - r_{AM}}\right) / (4 \times t_{squized\ SE} \times \sigma_{SE}) \times \left(r_{AM} + t_{squized\ SE}\right)^2$$

Here, σ_{SE} is the ionic conductivity of the SE [S/cm].

Supplementary Note 4. Calculation of electrode energy density of SSBs

To calculate the electrode energy density considering only the cathode side, which consists of the cathode and Al current collector, **Equation (11)** was used.

Equation (11):

$$Energy\ density_{Electrode} = \frac{2 \times Discharging\ capacity_{AM} \times Wt_{AM} \times Areal\ total\ loading_{cathode} \times Cell\ voltage}{\left(2 \times Areal\ total\ loading_{cathode} + (\frac{\rho_{Al} \times t_{Al}}{10})\right)}$$

Here, $Energy\ density_{Electrode}$ is the energy density of the electrode [Wh kg^{-1}]; $Discharging\ capacity_{AM}$ is the discharging capacity of the AM [Ah kg^{-1}]; Wt_{AM} is the weight ratio of the AM [wt%]; $Areal\ total\ loading_{cathode}$ is the areal total loading of the cathode [kg cm^{-2}], which can be calculated by multiplying the cathode loading thickness by the electrode density; ρ_{Al} is the density of the Al current collector [kg cm^{-3}]; and t_{Al} is the thickness of the Al current collector [cm].

To calculate the electrode energy density considering both the cathode and anode sides using graphite as the anode material, **Equation (12) and Equation (13)** were used.

Equation (12):

$$Energy\ density_{Electrode} = \frac{2 \times Discharging\ capacity_{AM} \times Wt_{AM} \times Areal\ total\ loading_{cathode} \times Cell\ voltage}{\left(2 \times Areal\ total\ loading_{cathode} + (\frac{\rho_{Al} \times t_{Al}}{10})\right) + \left(2 \times Areal\ total\ loading_{graphite} + (\frac{\rho_{Cu} \times t_{Cu}}{10})\right)}$$

Here, $Areal\ total\ loading_{graphite}$ is the areal total loading of graphite [kg cm^{-2}], which can be calculated using **Equation (13)**; ρ_{Cu} is the density of the Cu current collector [kg cm^{-3}]; and t_{Cu} is the thickness of the Cu current collector [cm].

Equation (13):

$$Areal\ total\ loading_{graphite} = \frac{Dischaging\ capacity_{AM}}{Dischaging\ capacity_{graphite}} \times \frac{N}{P} ratio \times Areal\ total\ loading_{cathode}$$

Here, $Discharging\ capacity_{AM}$ is the discharging capacity of the AM [Ah kg^{-1}], $Discharging\ capacity_{graphite}$ is the discharging capacity of graphite [Ah kg^{-1}], and N/P ratio is the areal capacity ratio of the negative to positive electrode.

To calculate the electrode energy density considering both the cathode and anode sides using Li metal instead of graphite as the anode material, **Equation (14)** was used.

Equation (14):

$$Energy\ density_{Electrode} = \frac{2 \times Discharging\ capacity_{AM} \times Wt_{AM} \times Areal\ total\ loading_{cathode} \times Cell\ voltage}{\left(2 \times Areal\ total\ loading_{cathode} + (\frac{\rho_{Al} \times t_{Al}}{10})\right) + \left(2 \times Areal\ total\ loading_{Li} + (\frac{\rho_{Cu} \times t_{Cu}}{10})\right)}$$

Here, $Areal\ total\ loading_{Li}$ is the areal total loading of Li [kg cm^{-2}].

To calculate the electrode energy density considering both the cathode and anode sides using Li metal as the anode material except with a Cu current collector, **Equation (15)** was used.

Equation (15):

$$Energy\ density_{Electrode} = \frac{2 \times Discharging\ capacity_{AM} \times Wt_{AM} \times Areal\ total\ loading_{cathode} \times Cell\ voltage}{\left(2 \times Areal\ total\ loading_{cathode} + (\frac{\rho_{Al} \times t_{Al}}{10})\right) + (2 \times Areal\ total\ loading_{Li})}$$

Supplementary Note 5. Calculation of energy density considering the electrode and SE of SSBs

To calculate the electrode energy density considering the electrode and SE, **Equation (16)** was used.

Equation (16):

$$Energy\ density_{Electrode+SE} = \frac{2 \times Discharging\ capacity_{AM} \times Wt_{AM} \times Areal\ total\ loading_{cathode} \times Cell\ voltage}{\left(2 \times Areal\ total\ loading_{cathode} + (\frac{\rho_{Al} \times t_{Al}}{10})\right) + \left(2 \times Areal\ total\ loading_{Li} + (\frac{\rho_{Cu} \times t_{Cu}}{10})\right) + (2 \times (\frac{\rho_{SE} \times t_{SE}}{10}))}$$

Here, $Energy\ density_{Electrode+SE}$ is the energy density of the electrode and SE [Wh kg^{-1}]; $Discharging\ capacity_{AM}$ is the discharging capacity of the AM [Ah kg^{-1}]; Wt_{AM} is the weight ratio of the AM [wt%]; $Areal\ total\ loading_{cathode}$ is the areal total loading of the cathode [kg cm^{-2}]; $Areal\ total\ loading_{Li}$ is the areal total loading of Li [kg cm^{-2}]; $Cell\ voltage$ is the nominal voltage [V]; ρ_{Al} is the density of the Al current collector [kg cm^{-3}]; t_{Al} is the thickness of the Al current collector [cm]; ρ_{Cu} is the density of the Cu current collector [kg cm^{-3}]; t_{Cu} is the thickness of the Cu current collector [cm]; ρ_{SE} is the density of the SE membrane [kg cm^{-3}]; and t_{SE} is the thickness of the SE membrane [cm].

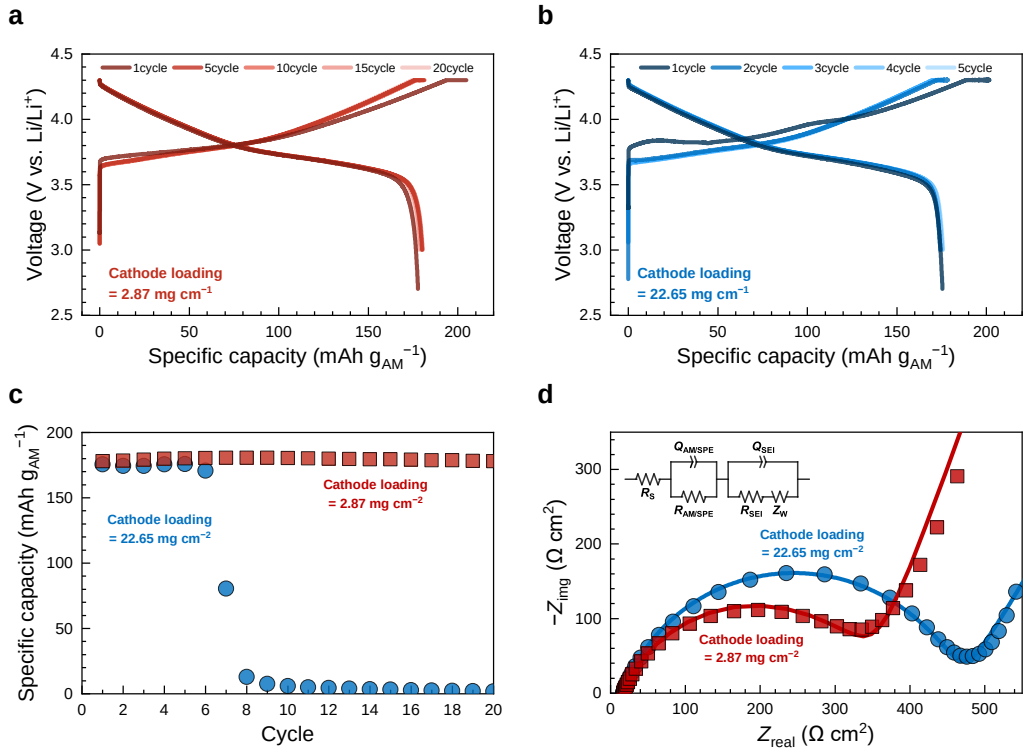

Supplementary Fig. 7: Coin-cell performance of SSBs based on SPE

a, Charge–discharge curves of Li/SPE/NCM622 coin cell with low cathode loading (3.50 mg cm^{-2}). **b,** Charge–discharge curves of Li/SPE/NCM622 coin cell with high cathode loading (22.67 mg cm^{-2}). **c,** Discharging capacity during cycling of Li/SPE/NCM622 coin cells with different cathode loading levels. **d,** EIS results of Li/SPE/NCM622 coin cells with different cathode loading levels.

To evaluate the cell performance of SSBs using the developed SPE and freestanding Li-metal anode design, coin-cell tests were performed to examine the effect of the areal cathode loading on the cell performance. The weight ratio of AM was 94 wt%, and the C-rate was 0.1 C for all the coin-cell tests. One coin cell had a low cathode loading of 3.50 mg cm^{-2}, and the other had a high cathode loading of 22.67 mg cm^{-2}.

The results of the cycling test indicated that the areal discharging capacity was 179.2 mAh g_{AM}^{-1} with the low areal cathode loading and 174.4 mAh g_{AM}^{-1} with the high areal cathode

loading, which are similar values. However, the discharging capacity and energy increased from 0.791 mAh and 3.01 mWh with the low areal cathode loading to 6.081 mAh and 23.18 mWh with the high areal cathode loading. This result indicates that a high areal cathode loading is necessary for producing high capacity and energy output of the SSBs.

The coulombic efficiency was similar for the low areal cathode loading (99.25%) and high areal cathode loading (99.20%). However, the energy efficiency was lower for the coin cell with high areal cathode loading (96.70%) than for that with the low areal cathode loading (99.25%). This result suggests a trade-off between the energy and energy efficiency depending on the areal cathode loading. The higher cathode IR drop with higher areal cathode loading results in low energy efficiency.

Capacity retention is also an essential parameter in cell performance. The coin cell exhibited stable capacity retention when using low areal cathode loading during 20 cycles. However, sudden capacity fading was observed after the 7^{th} cycle for the coin cell using high areal cathode loading. This result indicates that a high areal cathode loading induces a high IR drop, leading to the high resistance of the cell and capacity decay. The resistance of the cell before and after full-cell cycling was measured using EIS, and it increased as expected in calculating the cathode IR drop tendency depending on the areal cathode loading. In summary, both the anode and SPE showed good stability during cycling, and the capacity decay may stem from the increased resistance of the cell due to the high cathode IR drop when using high areal cathode loading.

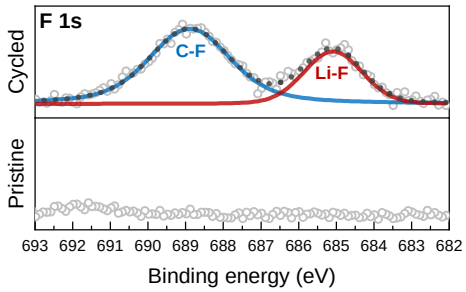

Supplementary Fig. 8: XPS data of Li-metal anode after full-cell cycling of Li/SPE/NCM622 coin cell.

After the full-cell cycling of the coin cell, XPS data of the Li-metal anode side was collected, and formation of C-F and LiF, stemming from the PVDF-HFP in the SPE, was observed. The LiF formed the stable layer on the Li-metal anode[S2].

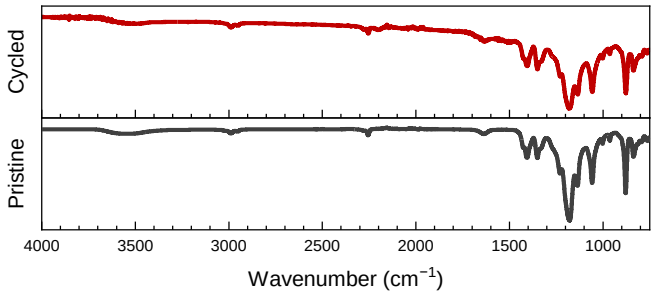

Supplementary Fig. 9: FTIR data of SPE before and after full-cell cycling of Li/SPE/NCM622 coin cell.

FTIR spectra of the SPE before and after full-cell cycling were analyzed and indicated no structural change during cycling.

Supplementary Table 1. Parameters for SSB pouch cell targeting energy density of 200 Wh kg^{-1}.

Electrode	**Li**	**NCM622**		**Electrolyte**	**N/A**	
Layers	6	4		True density	0.00	g cm^{-3}
Active materials capacity (charge, single-side)	-	207.74	mAh g^{-1}	Excess ratio	0.00	vol%
	-	3.69	mAh cm^{-2}	E/C ratio	0.00	g Ah^{-1}
Active materials capacity (discharge, single-side)	3860	187.14	mAh g^{-1}	Volume	0.00	cm^3
	4.12	3.32	mAh cm^{-2}	Weight	0.00	g
N/P (discharge)		2.35		**Separator**	**SPE**	
Initial coulombic efficiency		90.08	%	True density	1.80	g cm^{-3}
Nominal discharge voltage	0.00	3.81	V vs. Li/Li^+	Pore volume	0.00	cm^3
Active materials ratio	100.00	93.00	wt%	Porosity	0.00	vol%
Solid electrolyte ratio	0.00	5.00	wt%	Thickness	82.00	μm
Binder ratio	0.00	0.00	wt%	Width	3.40	cm
Conductive agent ratio	0.00	2.00	wt%	Height	4.55	cm
Areal total loading weight	1.07	19.09	mg cm^{-2}	Area	15.47	cm^2
Spatial total loading density	0.53	3.70	g cm^{-3}	Volume	0.13	cm^3
True total loading density	0.53	4.28	g cm^{-3}	Weight	0.23	g
Pore volume	0.00	0.01	cm^3	**Package**	**Al pouch**	
Porosity	0.00	13.64	vol%	Areal weight	180.00	g m^{-2}
Thickness	20.00	51.59	μm	Thickness	110.00	μm
Width	3.00	2.90	cm	Width	3.90	cm
Height	4.15	4.05	cm	Height	5.45	cm
Area	12.45	11.75	cm^2	Area	21.26	cm^2
Volume	0.02	0.06	cm^3	Volume	0.23	cm^3
Weight	0.01	0.22	g	Weight	0.38	g
Current collector	**Cu**	**Al**		**Cell dimension**		
Layers	3	2		Parallel stack	4	unit cell
True density	8.96	2.70	g cm^{-3}	Nominal discharge voltage	3.81	V
Thickness	0.00	20.00	μm	Discharge capacity	156.08	mAh
Width	3.00	2.90	cm	Width	3.90	cm
Height	4.15	4.05	cm	Height	5.45	cm
Area (+ tab)	0.40	12.15	cm^2	Thickness	0.87	mm
Volume	0.00	0.02	cm^3	Volume	1.43	cm^3
Weight	0.00	0.07	g	Weight	2.92	g
Lead tab	**Ni**	**Al**		**Energy density**	**203.64**	**Wh kg^{-1}**
Weight	98.30	36.90	mg		**416.09**	**Wh L^{-1}**

Supplementary Table 2. Parameters for SSB pouch cell targeting energy density of 280 Wh kg^{-1}.

Electrode	**Li**	**NCM622**		**Electrolyte**	**N/A**	
Layers	22	20		True density	0.00	g cm^{-3}
Active materials capacity (charge, single-side)	-	195.33	mAh g^{-1}	Excess ratio	0.00	vol%
	-	4.82	mAh cm^{-2}	E/C ratio	0.00	g Ah^{-1}
Active materials capacity (discharge, single-side)	3860	173.16	mAh g^{-1}	Volume	0.00	cm^3
	4.12	4.27	mAh cm^{-2}	Weight	0.00	g
N/P (discharge)		2.09		**Separator**	**SPE**	
Initial coulombic efficiency		88.65	%	True density	1.80	g cm^{-3}
Nominal discharge voltage	0.00	3.75	V vs. Li/Li^+	Pore volume	0.00	cm^3
Active materials ratio	100.00	94.00	wt%	Porosity	0.00	vol%
Solid electrolyte ratio	0.00	4.00	wt%	Thickness	96.00	μm
Binder ratio	0.00	0.00	wt%	Width	3.40	cm
Conductive agent ratio	0.00	2.00	wt%	Height	4.55	cm
Areal total loading weight	1.07	26.23	mg cm^{-2}	Area	15.47	cm^2
Spatial total loading density	0.53	3.70	g cm^{-3}	Volume	0.15	cm^3
True total loading density	0.53	4.35	g cm^{-3}	Weight	0.27	g
Pore volume	0.00	0.01	cm^3	**Package**	**Al pouch**	
Porosity	0.00	14.92	vol%	Areal weight	180.00	g m^{-2}
Thickness	20.00	70.90	μm	Thickness	110.00	μm
Width	3.00	2.90	cm	Width	3.90	cm
Height	4.15	4.05	cm	Height	5.45	cm
Area	12.45	11.75	cm^2	Area	21.26	cm^2
Volume	0.02	0.08	cm^3	Volume	0.23	cm^3
Weight	0.01	0.31	g	Weight	0.38	g
Current collector	**Cu**	**Al**		**Cell dimension**		
Layers	11	10		Parallel stack	20	unit cell
True density	8.96	2.70	g cm^{-3}	Nominal discharge voltage	3.75	V
Thickness	0.00	20.00	μm	Discharge capacity	1002.93	mAh
Width	3.00	2.90	cm	Width	3.90	cm
Height	4.15	4.05	cm	Height	5.45	cm
Area (+ tab)	0.40	12.15	cm^2	Thickness	4.16	mm
Volume	0.00	0.02	cm^3	Volume	6.25	cm^3
Weight	0.00	0.07	g	Weight	13.38	g
Lead tab	**Ni**	**Al**		**Energy density**	**281.19**	**Wh kg^{-1}**
Weight	98.30	36.90	mg		**602.06**	**Wh L^{-1}**

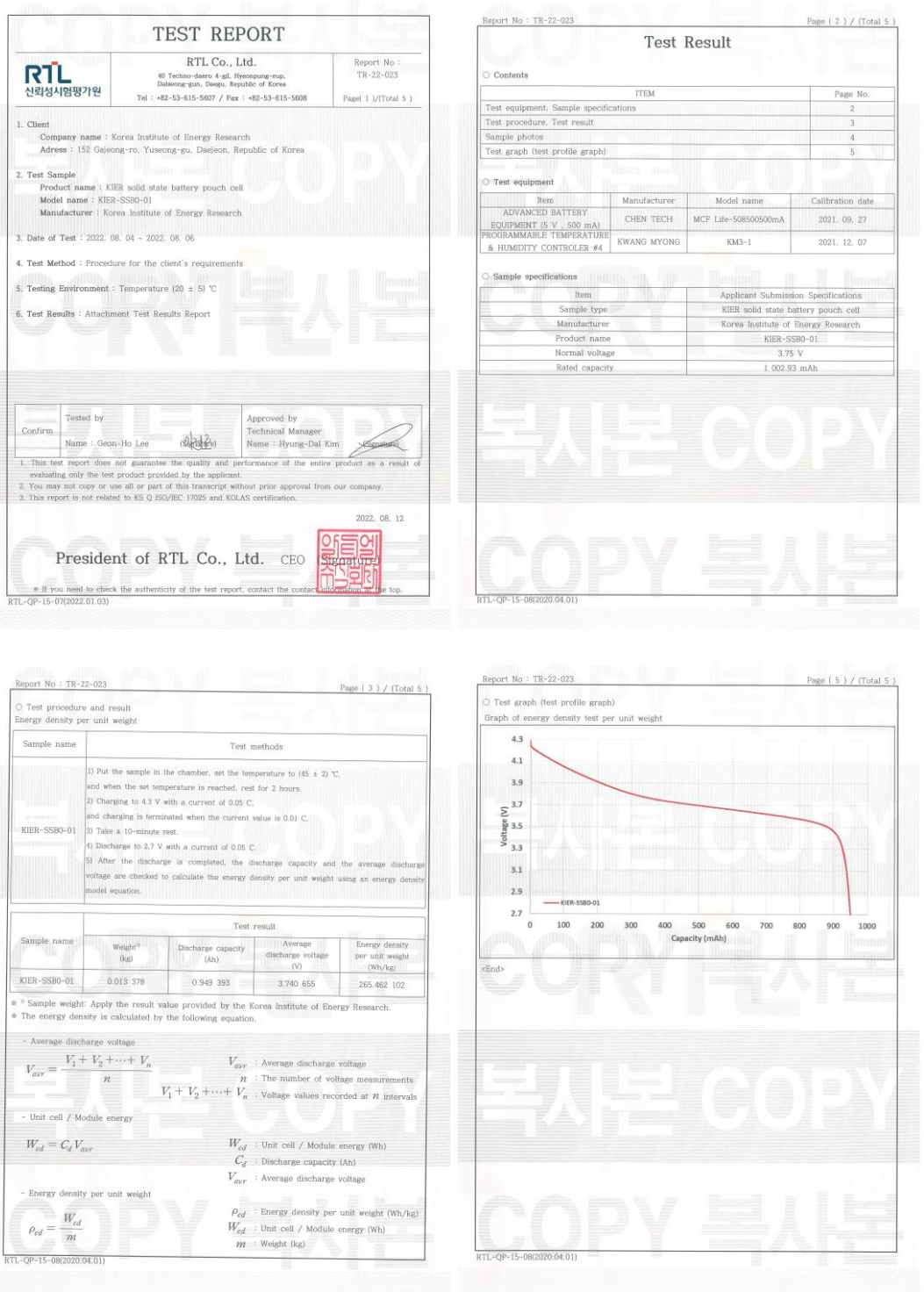

TEST REPORT

RTL Co., Ltd.
40 Techno-daero 4-gil, Hyeonpung-eup, Dalseong-gun, Daegu, Republic of Korea
Tel : +82-53-615-5607 / Fax : +82-53-615-5608

Report No : TR-22-023
Page(1)/(Total 5)

1. Client
Company name : Korea Institute of Energy Research
Adress : 152 Gajeong-ro, Yuseong-gu, Daejeon, Republic of Korea

2. Test Sample
Product name : KIER solid state battery pouch cell
Model name : KIER-SSB0-01
Manufacturer : Korea Institute of Energy Research

3. Date of Test : 2022. 08. 04 ~ 2022. 08. 06

4. Test Method : Procedure for the client's requirements

5. Testing Environment : Temperature (20 ± 5) ℃

6. Test Results : Attachment Test Results Report

Confirm	Tested by	Approved by
	Name : Geon-Ho Lee (Signature)	Technical Manager Name : Hyung-Dal Kim (Signature)

1. This test report does not guarantee the quality and performance of the entire product as a result of evaluating only the test product provided by the applicant.
2. You may not copy or use all or part of this transcript without prior approval from our company.
3. This report is not related to KS Q ISO/IEC 17025 and KOLAS certification.

2022. 08. 12

President of RTL Co., Ltd. CEO (Signature)

※ If you need to check the authenticity of the test report, contact the contact information at the top.

RTL-QP-15-07(2022.01.03)

Report No : TR-22-023
Page(2)/(Total 5)

Test Result

○ Contents

ITEM	Page No.
Test equipment, Sample specifications	2
Test procedure, Test result	3
Sample photos	4
Test graph (test profile graph)	5

○ Test equipment

Item	Manufacturer	Model name	Calibration date
ADVANCED BATTERY EQUIPMENT (5 V , 500 mA)	CHEN TECH	MCF Life-508500500mA	2021. 09. 27
PROGRAMMABLE TEMPERATURE & HUMIDITY CONTROLER #4	KWANG MYONG	KM3-1	2021. 12. 07

○ Sample specifications

Item	Applicant Submission Specifications
Sample type	KIER solid state battery pouch cell
Manufacturer	Korea Institute of Energy Research
Product name	KIER-SSB0-01
Normal voltage	3.75 V
Rated capacity	1 002.93 mAh

RTL-QP-15-08(2020.04.01)

Report No : TR-22-023
Page(3)/(Total 5)

○ Test procedure and result
Energy density per unit weight

Sample name	Test methods
KIER-SSB0-01	1) Put the sample in the chamber, set the temperature to (45 ± 2) ℃, and when the set temperature is reached, rest for 2 hours. 2) Charging to 4.3 V with a current of 0.05 C, and charging is terminated when the current value is 0.01 C. 3) Take a 10-minute rest. 4) Discharge to 2.7 V with a current of 0.05 C. 5) After the discharge is completed, the discharge capacity and the average discharge voltage are checked to calculate the energy density per unit weight using an energy density model equation.

Sample name	Test result			
	Weight* (kg)	Discharge capacity (Ah)	Average discharge voltage (V)	Energy density per unit weight (Wh/kg)
KIER-SSB0-01	0.013 378	0.949 393	3.740 655	265.462 102

※ * Sample weight: Apply the result value provided by the Korea Institute of Energy Research.
※ The energy density is calculated by the following equation.

- Average discharge voltage

$$V_{avr} = \frac{V_1 + V_2 + \cdots + V_n}{n}$$

V_{avr} : Average discharge voltage
n : The number of voltage measurements
$V_1 + V_2 + \cdots + V_n$: Voltage values recorded at n intervals

- Unit cell / Module energy

$$W_{ed} = C_d V_{avr}$$

W_{ed} : Unit cell / Module energy (Wh)
C_d : Discharge capacity (Ah)
V_{avr} : Average discharge voltage

- Energy density per unit weight

$$\rho_{ed} = \frac{W_{ed}}{m}$$

ρ_{ed} : Energy density per unit weight (Wh/kg)
W_{ed} : Unit cell / Module energy (Wh)
m : Weight (kg)

RTL-QP-15-08(2020.04.01)

Report No : TR-22-023
Page(5)/(Total 5)

○ Test graph (test profile graph)
Graph of energy density test per unit weight

<End>

RTL-QP-15-08(2020.04.01)

Supplementary Fig. 6: Certification of energy density of ~280 Wh kg^{-1} from the second cycle by external third-party organization

Supplementary Table 3. Comparison of pouch-cell performance of SSB between this work and other references.

Ref		AM content mg cm^{-2}	AM ratio wt%	SE ratio wt%	CA ratio wt%	Binder ratio wt%	Cathode loading weight mg cm^{-2}	SE loading weight mg cm^{-2}	Anode loading weight mg cm^{-2}	Total cell loading weight mg cm^{-2}	Specific discharge capacity mAh g^{-1}	Nominal discharge voltage V	Areal discharge capacity mAh cm^{-2}	Gravimetric energy density Wh kg^{-1}
J. Electrochem. Soc. 161, A1812–A1817 (2014)	R13	5.15	68.6	29.4	2.0	0.0	7.50	151.00	5.30	163.80	125.0	3.59	0.64	14.10
ACS Appl. Mater. Interfaces 10, 2556–2565 (2018)	R14	6.23	70.0	30.0	0.0	0.0	8.90	127.40	4.30	140.60	131.0	3.76	0.82	21.83
J. Electrochem. Soc. 159, A1120–A1124 (2012)	R15	3.77	37.7	56.6	5.7	0.0	10.00	200.00	39.00	249.00	120.0	3.85	0.45	6.99
J. Power Sources 389, 140–147 (2018)	R16	5.89	78.5	21.5	0.0	0.0	7.50	150.70	29.40	187.60	130.0	3.92	0.77	15.99
Solid State Ionics 296, 13–17 (2016)	R17	1.38	60.0	35.0	5.0	0.0	2.30	90.40	3.00	95.70	100.0	3.28	0.14	4.73
ACS Appl. Mater. Interfaces 10, 31404–31412 (2018)	R18	7.00	70.0	25.0	2.5	2.5	10.00	90.40	5.30	105.70	168.0	3.7	1.18	41.17
J. Power Sources 375, 93–101 (2018)	S3	29.30	79.2	19.5	1.3	0.0	37.00	7.50	27.00	71.50	120.0	3.57	3.52	175.58
J. Power Sources 375, 93–101 (2018)	S3	14.30	68.1	29.2	1.3	1.4	21.00	4.90	13.00	38.90	110.0	3.67	1.57	148.41
Sci. Rep. 8, 1212 (2018)	S4	15.93	76.2	19.0	1.9	2.9	20.90	13.90	21.50	56.30	122.0	3.51	1.94	121.13
J. Electrochem. Soc. 164, A2474–A2478 (2017)	R19	9.50	66.0	28.3	2.8	2.8	14.40	11.30	10.20	35.90	111.0	3.62	1.05	106.38
Nat. Energy 1, 16030 (2016)	R20	4.86	60.0	34.0	6.0	0.0	8.10	49.80	6.00	63.90	110.0	3.71	0.53	31.04
J. Phys. Chem. Lett. 9, 607–613 (2018)	S5	115.29	61.0	36.0	3.0	0.0	189.00	18.00	112.00	319.00	123.0	3.75	14.18	166.70
J. Power Sources 248, 943–950 (2014)	R21	6.78	60.0	35.0	5.0	0.0	11.30	52.70	11.30	75.30	121.0	3.59	0.82	39.11
Nano Lett. 17, 3013–3020 (2017)	R22	10.01	86.3	11.0	1.8	0.9	11.60	134.60	6.00	152.20	119.0	3.69	1.19	28.88
J. Am. Chem. Soc. 140, 16330–16339 (2018)	S6	34.30	70.0	30.0	0.0	0.0	49.00	133.00	81.00	263.00	89.0	2.11	3.05	24.49
J. Electrochem. Soc. 162, A646–A651 (2015)	R23	0.60	30.0	60.0	10.0	0.0	2.00	75.00	5.00	82.00	1640.0	1.94	0.98	23.28
Nano Lett. 16, 7148–7154 (2016)	R24	3.60	40.0	50.0	10.0	0.0	9.00	180.00	5.00	194.00	501.0	1.25	1.80	11.62
J. Mater. Chem. A 6, 12098–12105 (2018)	R25	5.72	45.0	50.0	5.0	0.0	12.70	191.10	5.00	208.80	550.0	1.45	3.14	21.83
ACS Appl. Mater. Interfaces 10, 22264–22277 (2018)	R26	9.90	45.0	25.0	15.0	15.0	22.00	101.00	18.00	141.00	102.0	1.13	1.01	8.09
ACS Appl. Mater. Interfaces 10, 22329–22339 (2018)	R27	7.00	50.0	50.0	0.0	0.0	14.00	263.00	11.00	288.00	116.0	3.91	0.81	11.02
ACS Appl. Mater. Interfaces 9, 9654–9661 (2017)	S7	60.75	75.0	15.0	10.0	0.0	81.00	15.00	5.00	101.00	155.0	3.11	9.42	289.95
Solid State Ionics 315, 65–70 (2018)	R28	6.00	60.0	30.0	10.0	0.0	10.00	23.00	11.00	44.00	165.0	3.68	0.99	82.80
Chem. Mater. 28, 4453–4459 (2016)	S8	11.70	90.0	10.0	0.0	0.0	13.00	24.00	5.00	42.00	136.0	3.85	1.59	145.86
Energy Storage Mater. 18, 31261–31264 (2018)	R29	7.39	67.2	28.8	2.0	2.0	11.00	16.00	6.00	33.00	139.0	3.73	1.03	116.14
Nano Lett. 15, 2671–2678 (2015)	S9	14.70	70.0	25.0	5.0	0.0	21.00	3.00	2.00	26.00	165.0	3.27	2.43	305.05
J. Power Sources 364, 191–199 (2017)	R30	5.20	65.0	20.0	15.0	0.0	8.00	2.00	5.00	15.00	152.0	3.4	0.79	179.16
Nat. Mater. 12, 452–457 (2013)	R31	4.80	60.0	32.0	8.0	0.0	8.00	8.00	5.00	21.00	162.0	3.38	0.78	125.16
Nat. Energy, 5, 299-308 (2020)	R7	29.28	81.3	14.4	2.9	1.4	36.00	4.62	0.27	40.89	215.0	3.75	6.30	577.42
Science, 373, 1494-1499 (2021)	S10	21.65	77.3	19.3	2.9	0.5	28.00	107.80	5.00	140.80	200.0	3.75	4.33	115.30
Nature, 601, 217-222 (2022)	S11	10.30	70.0	10.0	10.0	10.0	14.72	2.55	1.87	19.14	210.0	3.75	2.16	423.97
Nat. Energy, 7, 83-93 (2022)	R36	47.25	90.0	10.0	0.0	0.0	52.50	178.25	1.35	232.10	95.0	3.75	4.49	72.52
This work		24.66	94.0	4.0	2.0	0.0	26.23	17.51	1.07	44.81	173.2	3.75	4.27	357.54

Supplementary references

S1. Aliahmad, N., Shrestha, S., Varahramyan, K., & Agarwal, M. Poly (vinylidene fluoride-hexafluoropropylene) polymer electrolyte for paper-based and flexible battery applications. *AIP Adv*. **6**, 065206 (2016).

S2. Park, S., Jeong, S. Y., Lee, T. K., Park, M. W., Lim, H. Y., Sung, J., Cho, J., Kwak, S. K., Hong, S. Y. & Choi, N. S. Replacing conventional battery electrolyte additives with dioxolone derivatives for high-energy-density lithium-ion batteries. *Nat. Commun*. **12**, 838 (2021).

S3. Nam, Y. J., Oh, D. Y., Jung, S. H. & Jung, Y. S. Toward practical all-solid-state lithium-ion batteries with high energy density and safety: Comparative study for electrodes fabricated by dry-and slurry-mixing processes. *J. Power Sources* **375**, 93-101 (2018).

S4. Yamamoto, M., Terauchi, Y., Sakuda, A. & Takahashi, M. Binder-free sheet-type all-solid-state batteries with enhanced rate capabilities and high energy densities. *Sci. Rep*. **8**, 1212 (2018).

S5. Kato, Y., Shiotani, S., Morita, K., Suzuki, K., Hirayama, M. & Kanno, R. All-solid-state batteries with thick electrode configurations. *J. Phys. Chem. Lett*. **9**, 607-613 (2018).

S6. Kraft, M. A., Ohno, S., Zinkevich, T., Koerver, R., Culver, S. P., Fuchs, T., Senyshyn, A., Indris, S., Morgan, B. J. & Zeier, W. G. Inducing high ionic conductivity in the lithium superionic argyrodites Li6+ x P1–x Ge x S5I for all-solid-state batteries. *J. Am. Chem. Soc*. **140**, 16330-16339 (2018).

S7. Chen, R. J., Zhang, Y. B., Liu, T., Xu, B. Q., Lin, Y. H., Nan, C. W. & Shen, Y. Addressing the interface issues in all-solid-state bulk-type lithium ion battery via an all-

composite approach. *ACS Energy Lett*. **9**, 9654-9661 (2017).

S8. Wakayama, H., Yonekura, H. & Kawai, Y. Three-dimensional bicontinuous nanocomposite from a self-assembled block copolymer for a high-capacity all-solid-state lithium battery cathode. *Chem. Mater*. **28**, 4453-4459 (2016).

S9. Hovington, P., Lagacé, M., Guerfi, A., Bouchard, P., Mauger, A., Julien, C. M., Armand, M. & Zaghib, K. New lithium metal polymer solid state battery for an ultrahigh energy: nano C-LiFePO4 versus nano Li1. 2V3O8. *Nano Lett*. **15**, 2671-2678 (2015).

S10. Tan, D. H., Chen, Y. T., Yang, H., Bao, W., Sreenarayanan, B., Doux, J. M., Li, W., Lu, B., Ham, S. Y., Sayahpour, B., Scharf, J., Wu, E. A., Deysher, G., Han, H. E., Hah, H. J., Jeong, H., Lee, J., Chen, Z. & Meng, Y. S. Carbon-free high-loading silicon anodes enabled by sulfide solid electrolytes. *Science* **373**, 1494-1499 (2021).

S11. Lee, M. J., Han, J., Lee, K., Lee, Y. J., Kim, B. G., Jung, K. N., Kim, B. J. & Lee, S. W. Elastomeric electrolytes for high-energy solid-state lithium batteries. *Nature* **601**, 217-222 (2022).